ChemComm

COMMUNICATION

View Article Online
View Journal | View Issue

Cite this: *Chem. Commun.*, 2019, **55**, 13932

Received 11th August 2019,
Accepted 21st October 2019

DOI: 10.1039/c9cc06214a

rsc.li/chemcomm

Bipedal DNA walker mediated enzyme-free exponential isothermal signal amplification for rapid detection of microRNA†

Anyi Chen, Ying Zhuo, Yaqin Chai * and Ruo Yuan *

In this work, a bipedal DNA walker was employed to mediate an efficient enzyme-free exponential isothermal DNA signal amplification. On the basis of the bipedal DNA walker mediated enzyme-free exponential isothermal signal amplification, an electrochemiluminescence (ECL) biosensor was constructed for sensitive and rapid detection of microRNA (miRNA) with a limit of detection down to 0.24 fM and requiring less than 40 min.

Enzyme-free isothermal DNA amplification technology has attracted enormous interest in bioanalysis for the outstanding advantages of wide applicability, low cost, and easy operation.[1–4] Nevertheless, conventional enzyme-free isothermal strategies, such as catalytic hairpin assembly (CHA),[5,6] strand displacement reaction (SDR)[7–9] and hybridization chain reaction (HCR),[2,10] achieved only linear signal amplification, which urged researchers to seek more sensitive methods. Recently, enzyme-free exponential isothermal DNA signal amplification strategies came into view for their capacity of explosive amplification.[11,12] To realize a typical exponential isothermal DNA amplification, it was essential that the ssDNA initiator generated from a circuit could initiate another circuit in each amplification cycle.[13–15] However, in an enzyme-free assay, the initiator could not be synthesized in real-time, and thus it must be prepared in advance, and the prepared initiator should be well blocked to avoid false initiation of the amplification by free initiator. Nevertheless, the blocking procedure inevitably hindered the normal liberation of the initiator, which slowed the reaction rate and decreased the amplification efficiency. Therefore, improving the DNA reaction rate became the key to achieving efficient enzyme-free exponential isothermal signal amplification. Recent evidence showed that DNA walkers remarkably accelerated the DNA reactions as the reaction of DNA strands was restricted in a confined space during the DNA walking to increase the local concentration of the DNA strands.[16–19] Herein, a bipedal DNA walker was employed to rapidly liberate the blocked initiators from the track *via* strand displacement reaction-powered DNA walking, realizing efficient enzyme-free exponential isothermal signal amplification.

In this work, on the basis of the biped DNA walker mediated enzyme-free exponential isothermal signal amplification strategy, an ultrasensitive electrochemiluminescence (ECL) biosensor was constructed for microRNA (miR-21) detection. First, polyethyleneimine-tris(2,2′-bipyridine)ruthenium(II) complex (PEI-Ru) modified TiO_2 nanospheres were labeled with streptavidin (SA) as ECL signal probes (TiO_2@PEI-Ru@SA). The Y junction DNA structures composed of capture probe (CP), assistant probe (AP) and secondary target (ST) were fabricated on a Pt nanoparticle modified glassy carbon electrode to construct a 2D track for the bipedal DNA walker. Before the formation of the DNA walker, the secondary target was inhibited on the electrode surface by a stable Y junction structure. As illustrated in Scheme 1, through a typical catalytic hairpin assembly process, cyclic assembly of two hairpin probes (H1 and H2) was triggered by target miR-21 to form double-stranded DNAs with single stranded terminals as bipedal DNA walkers. Utilizing DNA synergistic hybridization, the two pedals of the DNA walker synchronously hybridized with two CPs on the electrode surface, displacing AP and ST from the Y junction DNA structures. CP exposed a toehold to hybridize with biotin-HP (biotin modified hairpin probe), releasing a pedal of the DNA walker. The released pedal further hybridized with another nearby CP, realizing autonomous DNA walking on the track. Meanwhile, ST was released from the Y junction DNA structures, which further triggered the assembly of H1 and H2 to produce bipedal DNA walkers, achieving enzyme-free exponential signal amplification. As a result, plenty of DNA walkers formed in the presence of target miR-21 and walked on the 2D track along with the fabrication of biotin-HP to achieve a biotin-HP modified electrode surface. Subsequently, TiO_2@PEI-Ru@SA were assembled onto the electrode surface by biotin-SA coupling. With the use of TiO_2 nanospheres as the co-reaction accelerator of the PEI-Ru ECL system, the TiO_2@PEI-Ru@SA exhibited strong ECL emission. Moreover, the

Key Laboratory of Luminescent and Real-Time Analytical Chemistry (Southwest University), Ministry of Education, College of Chemistry and Chemical Engineering, Southwest University, Chongqing 400715, China. E-mail: yqchai@swu.edu.cn, yuanruo@swu.edu.cn; Fax: +86 23 68253172; Tel: +86 23 68252277

† Electronic supplementary information (ESI) available: Experimental section, characterization and mechanism study. See DOI: 10.1039/c9cc06214a

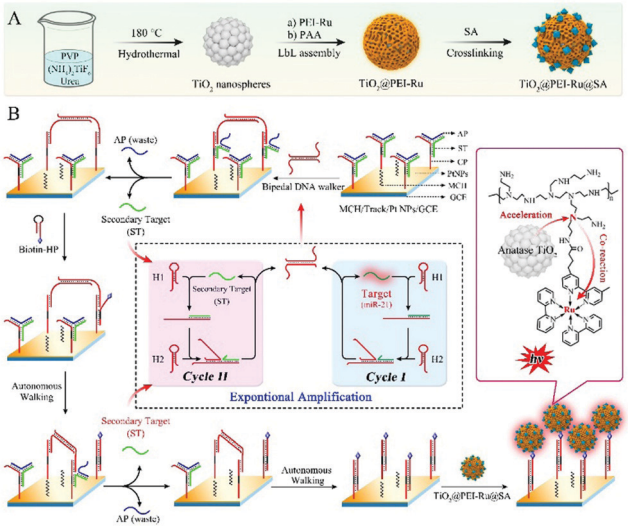

Scheme 1 Schematic illustration of the biosensor: (A) preparation of the ECL signal probes (TiO_2@PEI-Ru@SA) and (B) principle of the biosensor based on the bipedal DNA walker mediated enzyme-free exponential isothermal signal amplification for miR-21 detection.

bipedal DNA walkers accelerated the DNA strand displacement reactions, which greatly improved the efficiency of enzyme-free exponential isothermal signal amplification. The ECL biosensor proposed an enzyme-free method for rapid detection of nucleic acids, which possessed great application potential in clinical examination. More importantly, the strategy provided a powerful tool for signal amplification in the analysis of biomarkers.

Native polyacrylamide gel electrophoresis (PAGE) assay was employed to verify the formation of DNA walker response to miR-21. As shown in Fig. 1, three single bands assigned to H1, H2, and miR-21 were observed in lane 1, 2, and 3, respectively, which exhibited different migrations reverse to the numbers of bases. Lane 4, which loaded the mixture of H1, H2 and miR-21, exhibited a bright band with lower migration beyond the two bands of H1 and H2, manifesting the hybridization of H1 and H2. However, in lane 5, the PAGE image just displayed two distinct bands of H1 and H2 in the absence of miR-21, suggesting that the assembly of H1 and H2 was not permitted in the absence of miR-21. The PAGE result verified that target miR-21 could induce the generation of the bipedal DNA walkers.

Scanning electron microscopy (SEM) was employed to survey the morphology of the prepared nanomaterials. As shown in Fig. 2A, well-dispersed nanospheres could be observed in the field of vision with average diameter of 650 nm, indicating the successful preparation of TiO_2 nanospheres. The close-up of an individual particle clearly presented a lumpy surface, manifesting relatively large surface area of the TiO_2 nanospheres. Fig. 2B demonstrated the morphology of the TiO_2@PEI-Ru nanocomposites, which kept good dispersibility after the encapsulation of PEI-Ru. The close-up of an individual particle displayed a nanosphere covered with a cotton-like envelope, indicating that PEI-Ru was well immobilized on the TiO_2 nanospheres.

X-ray diffraction (XRD) was employed to survey the crystal pattern of the prepared TiO_2 nanospheres. As shown in Fig. 2C, typical diffraction peaks of the anatase phase of TiO_2 (JCPDS No. 21-1272)[20] were observed with the prepared TiO_2 nanospheres and no other characteristic peak was detected, indicating that anatase TiO_2 with high phase-purity was obtained in the synthesis. X-ray photoelectron spectra were measured for elemental analysis of the TiO_2@PEI-Ru nanocomposite. Fig. 2D depicted the full region of XPS for the TiO_2@PEI-Ru nanocomposites, which exhibited distinct peaks assigned to C1s, N1s, and O1s. High resolution XPS (Fig. 2E) displayed a distinct peak of $Ti2p_{3/2}$ at 457 eV, a slight peak of $Ru3p_{1/2}$ at 485 eV and a mixed peak of $Ti2p_{1/2}$ and $Ru3p_{3/2}$ at 463 eV, verifying the immobilization of PEI-Ru on TiO_2 nanospheres.

To confirm the fabrication of the ECL biosensor, CV experiments were carried out with different electrodes in 5.0 mM $[Fe(CN)_6]^{3-/4-}$ solution (Fig. 3A). Curve a displayed the typical redox peaks of $[Fe(CN)_6]^{3-/4-}$ with the bare GCE. After electrodepositing Pt NPs on the GCE surface, the redox current increased as Pt NPs increased the surface area of the electrode and accelerated the electron transfer (curve b). Then tracks (CP-AP-ST) were fabricated on the Pt NP modified electrode, and a remarkable decrease was observed with the redox current (curve c) because the Y junction

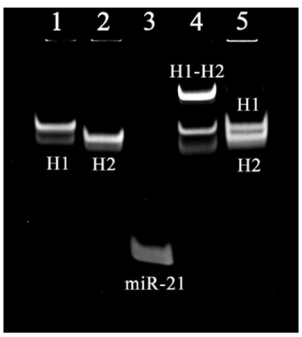

Fig. 1 Native PAGE images of different samples. Lane 1: H1 (1 μM); Lane 2: H2 (1 μM); Lane 3: miR-21 (2.5 μM); Lane 4: the mixture of H1 (1 μM), H2 (1 μM) and miR-21 (0.1 μM); Lane 5: the mixture of H1 (1 μM) and H2 (1 μM). All the samples were kept at room temperature for 1 h before PAGE assay.

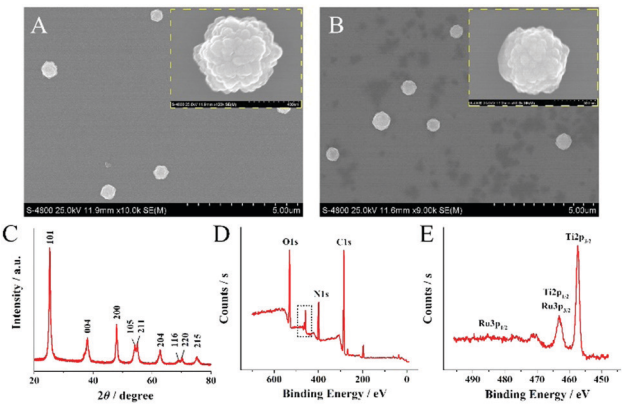

Fig. 2 (A) SEM images of the prepared TiO_2 nanospheres. (B) SEM images of the prepared TiO_2@PEI-Ru nanocomposite. The insets of A and B show a close-up of an individual particle with the scale bars of 400 nm and 500 nm, respectively. (C) XRD result of the TiO_2 nanospheres. (D) The full region and (E) high resolution spectra of XPS for the TiO_2@PEI-Ru nanocomposites.

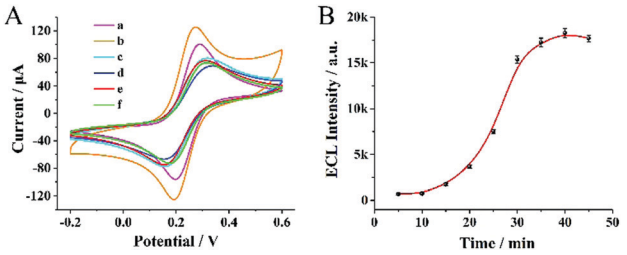

Fig. 3 (A) CVs at the bare GCE (a), Pt NPs/GCE (b), Tracks/Pt NPs/GCE (c), MCH/Tracks/Pt NPs/GCE (d), DNA walking/MCH/Tracks/Pt NPs/GCE (e), and TiO_2@PEI-Ru@SA/DNA walking/MCH/Tracks/Pt NPs/GCE (f). The CV experiments were implemented in 5.0 mM $[Fe(CN)_6]^{3-/4-}$ solution. (B) ECL response to different reaction times of the biosensor with 10 pM miR-21.

structure of the tracks significantly impeded the electron transfer. After blocking the nonspecific binding sites with MCH, the expanded impedance of the biosensor led to further decrease of the redox current (curve d). When the modified electrode was incubated with a mixture of H1, H2, biotin-HP and miR-21 to realize autonomous DNA walking on the track, the redox current was slightly increased (curve e). While the TiO_2@PEI-Ru@SA composite was assembled onto the modified electrode *via* biotin-SA binding, a slight decrease in redox current was observed (curve f) due to the nonconductivity of macromolecule SA. The results of the CV experiment verified the successful construction of the ECL biosensor for miR-21 detection, as expected.

To monitor the reaction process of the proposed enzyme-free exponential isothermal signal amplification and determine the optimized reaction time for miR-21 detection, the ECL intensity was measured with reaction time from 5 min to 45 min. As exhibited in Fig. 3B, the ECL intensity of the biosensor presented an increasing growth within 40 min, which was a typical characteristic of exponential amplifications.[15,21] After 40 min, the ECL intensity reached a maximum value. Therefore, 40 min was chosen as the reaction time for miR-21 detection.

To verify the capacity of the biosensor for miR-21 detection, standard miR-21 samples of different concentrations were measured by the prepared biosensor. As exhibited in Fig. 4A, only a weak ECL signal was achieved with the blank sample. While significant increases of the ECL intensity were observed when the concentration of miR-21 increased, verifying the response of the biosensor to miR-21. Moreover, the ECL responses showed a good linear relationship (correlation coefficient $r = 0.9984$) to the logarithmic

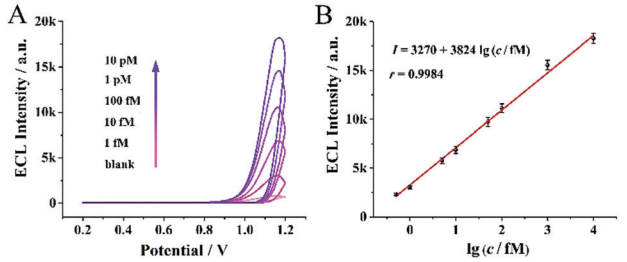

Fig. 4 (A) ECL responses of the biosensor to miR-21 at different concentrations. (B) Calibration plot showing the linear correlation between the ECL intensity and the logarithm of miR-21 concentration.

Table 1 The comparison for recent enzyme-free miRNA detection methods

Method	Time	LOD	Ref.
Fluorescence	1 h	8 pM	23
Electrochemistry	3 h	0.33 fM	24
SERS	4 h	0.17 fM	25
ECL	3 h	0.10 fM	26
ECL	2 h	1.51 fM	27
ECL	**40 min**	**0.24 fM**	**This work**

value of miR-21 concentrations ranging from 0.50 fM to 10 pM (Fig. 4B). The regression equation was $I = 3270 + 3824 \lg(c/\mathrm{fM})$ and the limit of detection (LOD) was calculated to be 0.24 fM.[22] Compared to recently reported enzyme-free miRNA detection methods, this biosensor achieved relatively low LOD and remarkably shortened the detection time (Table 1), manifesting the high efficiency of the bipedal DNA walker mediated enzyme-free exponential isothermal signal amplification.

The selectivity of the developed biosensor was tested by using three different miRNAs (miR-141, miR-155 and miR-199a) as interfering substances. As shown in Fig. 5A, these interfering miRNAs achieved very weak ECL intensities approximate to the blank in spite of the high concentrations (10 pM). However, miR-21 (100 fM) caused a remarkable ECL response, revealing the high specificity of the biosensor for miR-21 detection. Then, these interfering miRNAs (10 pM) were mixed with miR-21 (100 fM) to survey the influence on miR-21 detection. As expected, the mixture exhibited acceptable deviation compared to the ECL response of single miR-21. The results indicated that these interfering miRNAs influenced little the response to miR-21, manifesting good selectivity of the biosensor for the determination of miR-21.

The stability of a biosensor is an important indicator to evaluate its reliability in the measurement. To investigate the performance of the biosensor in the long testing process, the biosensor was continuously scanned in 0.1 M PBS (pH 7.4) for 20 cycles. Fig. 5B showed the ECL intensity of the biosensor to the scanning time, which exhibited average attenuation down to 0.32% in each cycle during continuous scanning, manifesting the favorable stability of the proposed biosensor.

To evaluate the feasibility of the proposed biosensor for tumor cell extraction analysis, the biosensor was employed to detect the expression of miR-21 in the extractions of human breast cancer cell line MCF-7 and human cervical cancer cell line HeLa. After the cell concentrations was set as 10 cells to 10^5 cells, the nucleic acids were extracted from the cells by a

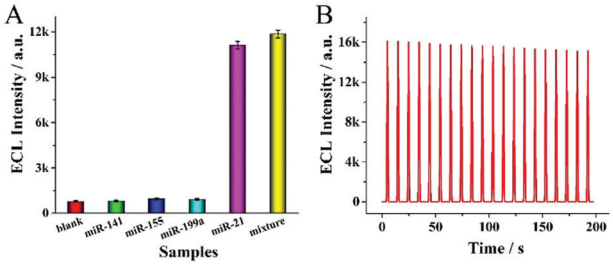

Fig. 5 (A) ECL response of the biosensors to different samples. (B) ECL performance of the biosensor under continuous scanning for 20 cycles.

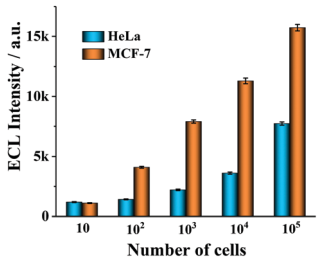

Fig. 6 ECL responses of the biosensor to HeLa and MCF-7 at different concentrations ranging from 10 cells to a hundred thousand cells.

conventional phenol chloroform extracting method. Then, the obtained solution was processed with a commercial column type miRNA extraction kit for ultimate extractions. As shown in Fig. 6, the extractions of MCF-7 cells caused a much stronger ECL response than HeLa cells at the same concentration, revealing the higher expression level of miR-21 in MCF-7 cells than HeLa cells. This result was well corresponding to recent reports,[25,28] suggesting the good feasibility of the ECL biosensor to determine the expression level of miRNA in cancer cells.

In summary, a bipedal DNA walker mediated enzyme-free exponential isothermal signal amplification strategy was proposed and applied to an ECL biosensor for rapid miR-21 detection. The bipedal DNA walker presented powerful capacity in accelerating the DNA reactions thus improving the efficiency of signal amplification. Benefiting from the efficient exponential isothermal signal amplification, the biosensor achieved rapid and sensitive detection of miR-21. Meanwhile, as an enzyme-free protocol, this method possessed good applicability to enzyme inhibitors in clinical samples, which exhibited a great application potential in clinical examination. Moreover, the work provided an example of using a DNA walker to improve the efficiency of complicated DNA reaction systems, which was inspiring to design efficient DNA signal amplification for sensitive bioanalysis.

This work was financially supported by the National Natural Science Foundation of China (21775124, 21575116, and 21675129) and the Fundamental Research Funds for the Central Universities, China (XDJK2017A001).

Conflicts of interest

There are no conflicts to declare.

Notes and references

1 S. Z. Yue, X. Y. Song, W. L. Song and S. Bi, *Chem. Sci.*, 2019, **10**, 1651–1658.
2 G. L. Xu, H. Zhoa, J. Reboud and J. M. Cooper, *ACS Nano*, 2018, **12**, 7213–7219.
3 K. Guk, S. G. Hwang, J. Lim, H.-Y. Son, Y. Choi, Y.-M. Huh, T. Kang, J. Jung and E.-K. Lim, *Chem. Commun.*, 2019, **55**, 3457–3460.
4 F. A. Wang, J. Elbaz and I. Willner, *J. Am. Chem. Soc.*, 2012, **134**, 5504–5507.
5 H. Cui, B. Bo, J. Ma, Y. Tang, J. Zhao and H. Xiao, *Chem. Commun.*, 2018, **54**, 4870–4873.
6 B. L. Li, A. D. Ellington and X. Chen, *Nucleic Acids Res.*, 2011, **39**, e110.
7 N. Zhang, X. M. Shi, H. Q. Guo, X. Z. Zhao, W. W. Zhao, J. J. Xu and H. Y. Chen, *Anal. Chem.*, 2018, **90**, 11892–11898.
8 Z. Zhang, D. D. Zeng, H. W. Ma, G. Y. Feng, J. Hu, L. He, C. Li and C. H. Fan, *Small*, 2010, **6**, 1854–1858.
9 Y. S. Hun, H. W. Li and J. B. Li, *J. Electroanal. Chem.*, 2018, **822**, 66–72.
10 J. Ge, C. Li, Y. Zhao, X. Yu and G. Jie, *Chem. Commun.*, 2019, **55**, 7350–7353.
11 C. P. Ma, M. H. Zhang, S. Chen, C. Liang and C. Shi, *Analyst*, 2016, **141**, 2883–2886.
12 M. Oishi, *ACS Omega*, 2018, **3**, 3321–3329.
13 M. S. Reid, X. C. Le and H. Q. Zhang, *Angew. Chem., Int. Ed.*, 2018, **57**, 11856–11866.
14 Y. Gao and B. Li, *Anal. Chem.*, 2014, **86**, 8881–8887.
15 H. X. Jia, Z. P. Li, C. H. Liu and Y. Q. Cheng, *Angew. Chem., Int. Ed.*, 2010, **49**, 5498–5501.
16 F. Chen, J. Xue, M. Bai, J. Qin and Y. X. Zhao, *Chem. Sci.*, 2019, **10**, 3103–3109.
17 K. W. Ren, Y. F. Xu, Y. Liu, M. Yang and H. X. Ju, *ACS Nano*, 2018, **12**, 263–271.
18 C. Jung, P. B. Allen and A. D. Ellington, *Nat. Nanotechnol.*, 2016, **11**, 157–163.
19 C. Jung, P. B. Allen and A. D. Ellington, *ACS Nano*, 2017, **11**, 8047–8054.
20 J. R. Huang, H. B. Ren, X. S. Liu, X. X. Li and J. J. Shim, *Superlattice Microstruct.*, 2015, **81**, 16–25.
21 J. Van Ness, L. K. Van Ness and D. J. Galas, *Proc. Natl. Acad. Sci. U. S. A.*, 2003, **100**, 4504–4509.
22 G. L. Long and J. D. Winefordner, *Anal. Chem.*, 1983, **55**, 712A–724A.
23 C. P. Liang, P. Q. Ma, H. Liu, X. G. Guo, B. C. Yin and B. C. Ye, *Angew. Chem., Int. Ed.*, 2017, **56**, 9077–9081.
24 L. Zhou, Y. Wang, C. Yang, H. Xu, J. Luo, W. Q. Zhang, X. Q. Tang, S. Yang, W. L. Fu, K. Chang and M. Chen, *Biosens. Bioelectron.*, 2019, **126**, 657–663.
25 X. X. Li, S. J. Ye and X. L. Luo, *Chem. Commun.*, 2016, **52**, 10269–10272.
26 L. P. Lu, J. X. Wang, W. J. Miao, X. Y. Wang and G. S. Guo, *Anal. Chem.*, 2019, **91**, 1452–1459.
27 L. C. Peng, P. Zhang, Y. Q. Chai and R. Yuan, *Anal. Chem.*, 2017, **89**, 5036–5042.
28 J. Zheng, J. H. Bai, Q. F. Zhou, J. S. Li, Y. H. Li, J. F. Yang and R. H. Yang, *Chem. Commun.*, 2015, **51**, 6552–6555.